An impedimetric immunosensor for the selective detection of CD34^{+} T-cells in human serum

Ana Díaz-Fernández[1,2], Elena Bernalte[1,2], Carlos Fernández-Ramos[1], Sandhya Moise[1,2], Pedro Estrela[2,3], Mirella Di Lorenzo[1,2,*]

[1] Department of Chemical Engineering, University of Bath, Bath, BA2 7AY, UK

[2] Centre for Biosensors, Bioelectronics and Biodevices (C3Bio), University of Bath, BA2 7AY, Bath, UK

[3] Department of Electronic and Electrical Engineering, University of Bath, BA2 7AY, Bath, UK

***** Corresponding author: m.di.lorenzo@bath.ac.uk

Graphical Abstract

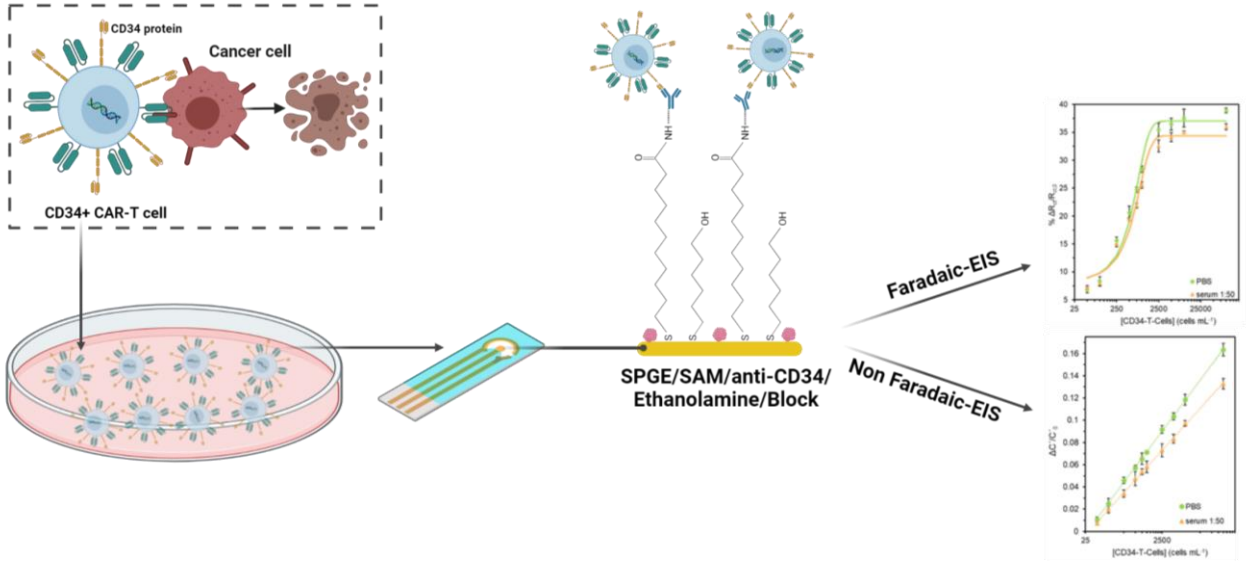

Abstract

Chimeric antigen receptor T (CAR-T) cell therapy has led to a paradigm change in cancer treatment. To allow widespread use of this therapy, it is important to reduce the costs associated with cells manufacturing whilst ensuring a high-quality production. Online biosensors can help monitor in real time the effectiveness of engineering CAR-T cells, with the possibility to be integrated on the workflow without the need to extract samples for off line analysis that require specialised personnel and expensive analytical equipment. In this context, we present an innovative label-free impedimetric immunosensor for the detection of $CD34^+$ T-cells in human serum. The sensor is based on screen printed gold electrodes functionalised with anti-CD34 antibody, via a mixed self-assembly monolayer of 11-mercaptoundecanoic acid and 6-mercapto-1-hexanol, which recognizes the CD34 antigen expressed onto the T-cells surfaces. The immunosensor exhibits a high selectivity and a wide working range in human serum, both in Faradaic and non-Faradaic detection conditions, being respectively of 230 – 1.4 x 10^3 cell mL^{-1} and 50 – 1 x 10^5 cell mL^{-1}. This result, along with performance validation both in batch and flow-through operations, demonstrates its applicability for clinical use.

Keywords

Electrochemical Biosensor, $CD34^+$ T-cells, Impedance, Capacitance, Flow-through Biosensor.

1. Introduction

Cancer is the second leading cause of death globally [1]. In 2018, leukaemia alone, a malignant disorder that provokes an increased number of leukocytes in the blood and/or bone marrow, costed 309,000 deaths worldwide [2]. Recently, Chimeric Antigen Receptor T (CAR-T) cell-based immunotherapy, which combines the specificity of antibodies to their antigens and the cytotoxic potential of T-cells, has shown great potential as an effective strategy for personalized cancer treatment [3]. This therapy, approved by the US Food and Drug Administration (FDA) and European Medicines Agency (EMA), has in particular shown clinical efficacy for acute lymphoblastic leukaemia, chronic lymphocytic leukaemia, and non-Hodgkin's lymphoma [4–6].

CAR-T cells are manufactured by genetically engineering patients' native T-cells *ex vivo*, to specifically recognize tumour antigens [7]. For example, CAR-T cells modified to express the glycosylated transmembrane protein CD34, can be used to reconstitute the complete hematopoietic system in patients affected by blood cancer [8]. One of the critical steps in the manufacturing process is the efficient isolation, quantification, and characterization of the functionalised T-cells. Flow cytometry is the gold standard technique for that purpose, but it suffers from limitations such as lack of standardization in assays, instrument setup, laborious sample preparation, and expensive equipment and reagents [9]. Biosensors would instead allow in-line, on-line and/or at-line monitoring of T-cell functionalisation in manufacturing, providing real time feedback, with excellent selectivity and sensitivity and no need for specialised personnel and equipment. This in turn can ultimately favour a wide application of CAR-T cell therapy by ensuring effective quality control while reducing overall manufacturing costs [10,11]. In particular, electrochemical biosensors such as impedimetric biosensors,

based on either a Faradaic or non-Faradaic detection, have great potential for real-time, label-free, and non-invasive detection of T-cells [12,13]. While Faradaic-based detection is indirect and requires the presence of a redox probe in solution limiting practical implementations, non-Faradaic (or capacitive) detection allows direct measurement of the target molecule in the sample, thus simplifying the operation [14,15]. Nevertheless, only a few electrochemical biosensors have been developed so far for T-cells detection, and to the best of our knowledge, none of them is for $CD34^+$ T-cells [9].

In this study, we propose an innovative impedimetric biosensor for the selective detection of $CD34^+$ T-cells in diluted human serum, which is the first electrochemical sensor developed for this type of T-Cells. The biosensor is based on screen-printed gold electrodes functionalised with anti-CD34 antibody, used as the recognition element, via a self-assembled monolayer approach. The ability of the biosensor to selectively detect $CD34^+$ T-cells is tested under both a Faradaic and non-Faradaic impedance modes, against other types of cells. The sensor is integrated into a microfluidic to demonstrate application in both static and flow-through mode.

2. Materials and methods

2.1 Materials

Monoclonal anti-CD34 antibody (QBEND10) was purchased from Invitrogen (Thermo Fisher, UK). Recombinant human CD34 (ab126924) and recombinant human CD44 (ab173996) proteins were obtained from Abcam (UK). Sulphuric acid (95-98 %), 11-mercaptoundecanoic acid, 6-mercapto-1-hexanol, N-(3-Dimethylaminopropyl)-N′-ethylcarbodiimide hydrochloride (EDC), N-hydroxysuccinimide (NHS), phosphate buffered saline tablets (PBS), ethanolamine hydrochloride, human serum from human

male AB plasma, bovine serum albumin (BSA), potassium hexacyanoferrate (III), potassium hexacyanoferrate (II) trihydrate and methanol were purchased from Merck (UK). MES buffered saline pack (pH 4.7), starting block® solution, potassium chloride, fetal bovine serum (FBS) media (Gibco), mammalian cell culture media IMDM (Gibco) and Hoechst 33342 stock solution were obtained from Thermo Fisher (UK). Purified anti-human CD34 Antibody, Mouse IgG1 kappa isotype, Clone MG1-45, and APC anti-mouse IgG1 antibody Clone RMG1-1 were purchased from BioLegend (UK). All the aqueous solutions were prepared with ultrapure water (18.2 MΩ cm^{-1}) from a Milli-Q system (Millipore, UK).

2.2 Apparatus

Electrochemical measurements were performed using a PalmSens4 potentiostat connected to a computer with PSTrace 5.7 software (PalmSens, The Netherlands). Screen-printed gold electrodes (DRP-C223BT), with a 1.6 mm gold working electrode, a gold counter electrode, and a silver pseudo-reference electrode, were purchased from Methrom Dropsens, UK.

The several functionalisation steps of the gold electrodes were monitored by cyclic voltammetry (CV) performed in a 50 µL drop of an electrolyte solution containing 5 mM $[Fe(CN)_6]^{3-}$, 5 mM $[Fe(CN)_6]^{4-}$ redox probe and 0.1 M KCl in 1x PBS buffer. The CV tests involved one potential cycle between -0.3 V and +0.7 V versus the Ag screen printed pseudo-reference electrode, at a scan rate of 100 mV s^{-1}.

Faradaic electrochemical impedance spectroscopy (EIS) measurements were performed in a solution containing 5 mM $[Fe(CN)_6]^{3-}$, 5 mM $[Fe(CN)_6]^{4-}$ and 0.1 M KCl in PBS buffer at 0.1345 V versus the Ag pseudo-reference electrode, which corresponds to the formal potential of the redox couple (measured by cyclic voltammetry). EIS frequency was varied within the range 0.1 Hz - 10 kHz with an amplitude of 10 mV. In

order to account for possible electrode-to-electrode variations and to normalize the obtained signals, changes in charge transfer resistance, R_{ct}, among different electrodes and for different days of operation, were expressed as the percentage of change with respect to the initial value for the sensing phase in the absence of the target protein ($R_{ct,0}$).

The capacitive EIS (non-Faradaic) measurements were performed in 1x PBS buffer at an equilibrium potential of 0 V versus the Open Circuit Potential (OCP), by applying an amplitude voltage of 50 mV a.c. within the frequency range 0.1 Hz - 10 kHz. The 'complex' capacitance of the system was calculated from the impedance spectra using Equations (1) and (2):

$$C' = - Z'' / \omega \cdot |Z|^2 \quad (1)$$

$$C'' = - Z' / \omega \cdot |Z|^2 \quad (2)$$

Where: Z'' is the imaginary part of the impedance; Z' the real part of the impedance; $|Z|^2 = (Z'^2)+(Z''^2)$; and ω is the phase angle.

2.3 Cell culture

Primary human peripheral blood $CD34^+$ cells (StemCell Technologies, Canada) as non-adherent cells, were expanded in suspension in a humidified atmosphere at 37 °C and 5% CO_2 in proliferation media for 14 days and harvested at days 7 and 14. Proliferation media was composed of StemSpan™ SFEM II medium supplemented with 10% StemSpan™ CD34 Expansion Supplement, 1 μM UM729 (all from StemCell Technologies, UK). At day 7, the cells were split, and one part reseeded in proliferation media and the remaining cells used for further analysis. Cell numbers were counted using a NucleoCounter® (Chemometec, Denmark) image cytometer.

HL-60 human promyeloblasts cells (ATCC CCL-240; LGC standard, UK) as non-adherent cells, were cultivated in suspension in a humidified atmosphere at 37 °C

and 5% CO_2 in proliferation media. The proliferation media was composed of RPMI-1640 medium (Sigma-Aldrich, UK) supplemented with 20% foetal bovine serum (Fisher Scientific, UK), 1% v/v Penicillin-Streptomycin (Fisher Scientific, UK) and 1% v/v Glutamax (Fisher Scientific, UK). The cell culture media was changed every two or three days, and the cells were passaged once per week to maintain a cell concentration of approximately 5×10^4 - 1.5×10^5 cells mL^{-1}.

The murine myoblast cell line C2C12 (ATCC, USA) as adherent cells, were expanded as monolayers on tissue culture plastic in a humidified atmosphere at 37 °C and 5% CO_2 in proliferation media. Proliferation media consisted of high glucose Dulbecco's Modified Eagle's Medium (Sigma-Aldrich, UK) supplemented with 10% v/v foetal bovine serum (Thermo Fisher Scientific, UK) and 1% v/v Penicillin - Streptomycin (Sigma-Aldrich, UK). Cells were passaged once every 72 hours when they reach ~80% confluence.

Prior to further testing, cells were fixed with 70% ice cold methanol for 5 min at room temperature. Excess methanol was washed and cells either stored for biosensor analysis or further stained for flow cytometric analysis.

2.4 Flow cytometry analysis

The presence of the CD34 signalling membrane protein for the peripheral blood $CD34^+$ cells, HL-60 and C2C12 cells was investigated by flow-cytometry. Fixed cells were blocked with 1% w/v bovine serum albumin (Sigma, UK), to avoid non-specific binding of antibodies, followed by labelling with anti-human CD34 antibody (Biolegend, UK) at 1:50 dilution. Unlabelled and mouse IgG1, κ isotype control (Biolegend, UK) antibody were prepared as assay controls. Following a 30 min incubation at room temperature, excess stains were washed off and the cells incubated with the secondary fluorophore label (except to the unlabelled control sample). APC

anti-mouse IgG1 Antibody (Biolegend, UK) was added to the cells at 1:500 dilution and incubated for 30 min at room temperature in dark. Secondary label was washed off and cells stained with Hoechst (Thermo Fisher, UK) at a 1 mg mL^{-1} and analysed immediately using a FACS Aria (BD Biosciences, UK) flow cytometer. Live cells were gated in the FSC vs SSC plot followed by FSC vs Hoechst plots. $CD34^{+}$ gate was set to include < 2% of the IgG1 sample to account for background staining.

2.5 Immunosensor fabrication

Prior to be used, the gold screen-printed electrodes were cleaned with ethanol and distilled water, dried with nitrogen, and then electrochemically cleaned by applying 10 potential cycles between 0 V and +1.3 V at a scan rate of 100 mV s^{-1} in 50 µL drop of 50 mM H_2SO_4. The electrodes were then rinsed with distilled water and dried with nitrogen.

The functionalisation of the gold screen-printed electrodes was performed by following the steps illustrated in Figure 1. First, to build a mixed self-assembled monolayer (SAM) on the gold surface, the electrodes were incubated with a 1:3 solution of 11-mercaptoundecanoic acid (MUA) and 6-mercapto-1-hexanol (MH), both 1 mM in MES buffer (pH 4.7). The incubation was carried out overnight at 4 °C and under a wet atmosphere to avoid possible evaporation. Then, the carboxylic groups immobilised on the surface were subsequently activated with a mixture of 100 mM EDC and 25 mM NHS in MES buffer for 30 min. The so-modified electrodes were then incubated with 10 µg mL^{-1} of anti-CD34 antibody in PBS buffer (1x, pH 7.4) for 30 min. The remained active groups after the antibody immobilisation were blocked with a 1 mM solution of ethanolamine in PBS for 15 min. Finally, the electrode surface was blocked with the starting block® solution for 30 min.

All these steps were performed in a total volume of 2 µL at room temperature. After each modification step, the electrode was rinsed with the buffer of the following step and gently dried with nitrogen.

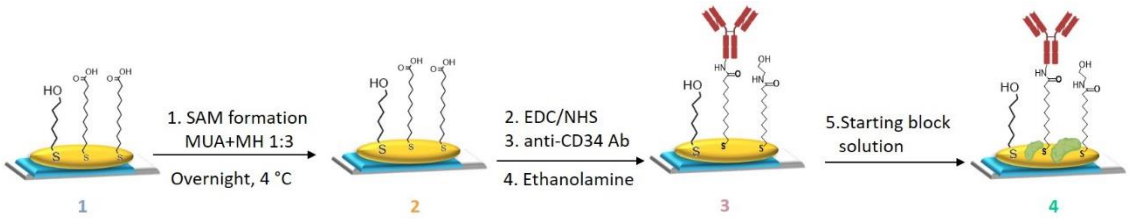

Figure 1: Steps of the construction of the impedimetric immunosensor for $CD34^+$ T-cells detection based on the immobilization of anti-CD34 antibody.

2.6 Protein and cells detection tests

First, impedimetric detection tests were performed with the purified protein CD34. Solutions of different concentrations of CD34 protein were prepared in PBS buffer from the stock solution (1 mg mL^{-1}). Afterwards, similar electrochemical tests were performed with T-cells expressing the CD34 marker; tests with HL-60 and C2C12 cells, which do not express CD34, were also performed to confirm the sensor selectivity. $CD34^+$ T-cells, HL-60 cells, and C2C12 cells solutions were prepared by serial dilution of the fixed cells, either in PBS or in human serum. Different dilutions of the serum with PBS were tested within the range 1:0 (undiluted) to 1:50. Each test was performed by incubating the modified Au electrodes with 2 µL of a solution of either the CD34 protein or the cells for 30 min at room temperature. After each incubation, the electrode was rinsed with PBS, dried with nitrogen, and the Faradaic or non-Faradaic EIS was recorded. In the case human serum, to compensate for the effect of non-specific interactions, the sensor was preincubated with human serum diluted 1:50 without cells,

and the value of the impedance obtained after this conditioning step was used as a reference.

Additionally, continuous flow measurements were performed in a microfluidic flow cell (drp-flwcl, Methrom Dropsens, UK), under a flow rate of 12 µL min^{-1} by means of a BT100-2J peristaltic pump (LongerPump, China) and 1.6 mm inner diameter tubes. The flow cell reactor was designed to obtain an inlet flow perpendicular to the electrode surface with an outlet flow at an angle of 45°. First, the samples were fed through the system for 30 min, followed by PBS for 5 min. Afterwards, the capacitive EIS was measured in PBS under the same flow conditions.

3 Results and discussion

Each modification step of the gold screen printed electrodes with the SAM and the anti-CD34 antibody was monitored by electrochemical impedance spectroscopy and cyclic voltammetry. The results shown in Figure 2 confirm a correct fabrication of the immunosensor. As shown in Figure 2A, the charge transfer resistance, R_{ct}, of the screen-printed gold increases after the formation of the SAM from 0.560 ± 0.082 kΩ to 31 ± 5 kΩ. This result is a consequence of the formation of a highly compact carbon chain and the negative charge of the carboxylic groups of the SAM that create an electrostatic barrier to the negatively charged redox markers and hence hinder the electron transfer. After the carboxylic acid activation with EDC and NHS, the antibody immobilisation, and the blocking with ethanolamine, R_{ct} decreased to 9 ± 2 kΩ, due to the removal of the negative charges on the SAM resulting from the binding of the antibody to the carboxylic groups. After blocking the so-modified electrode surface with the starting block® solution, a slight increase in R_{ct} (11 ± 2 kΩ) was observed, because of the blocking of the surface that enhanced the surface resistance. The CV

tests confirm the results from the EIS analysis (Figure 2B, Table 1); the SAM formation caused a decrease in the oxidation and reduction current peaks and a bigger difference between the oxidation and reduction peaks potential (ΔE_p). With the antibody immobilisation, followed by the surface blocking, the oxidation and reduction current increased and ΔE_p decreased.

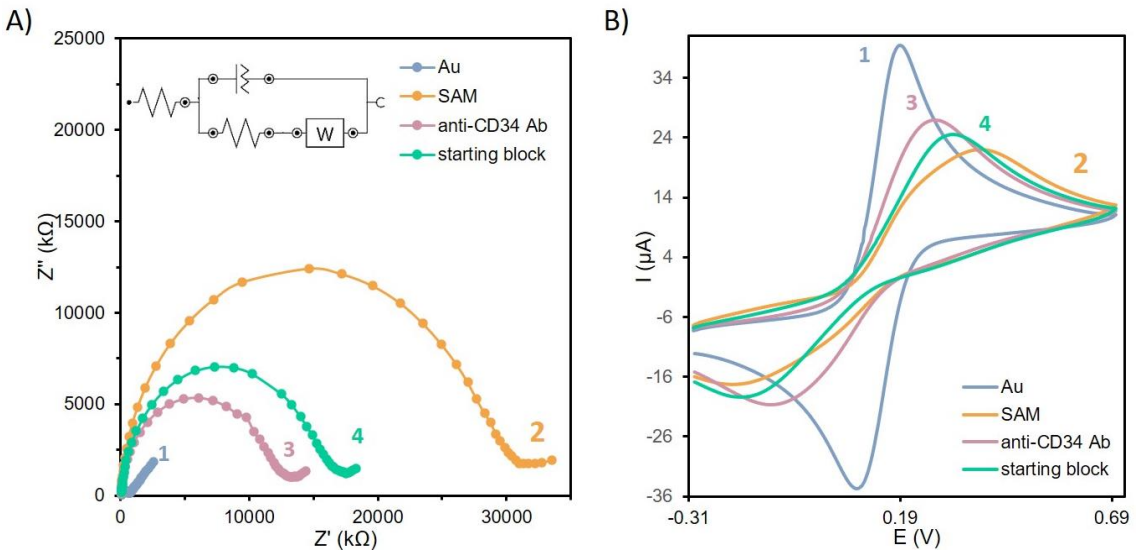

Figure 2: A) Nyquist plot from Faradaic EIS measurements in 5 mM $Fe[(CN)_6]^{3-/4-}$ after each step of fabrication, with a Randle's circuit used to fit the data. B) Cyclic voltammograms obtained after each step of fabrication, performed in 5 mM $Fe[(CN)_6]^{3-/4-}$ between -0.3 V and +0.7 V vs. Ag pseudo-reference electrode at a scan rate of 100 mV s^{-1}

Table 1. R_{ct} values and oxidation and reduction peaks potentials (vs. Ag pseudo-reference electrode) after each step of fabrication of the immunosensor

Fabrication step	**R_{ct} value (kΩ)**	**E_{ox} peak (V)**	**E_{red} peak (V)**
Bare gold	0.56 ± 0.08	0.191	0.087
SAM	31 ± 5	0.381	-0.208
Anti-CD34 Ab	9 ± 2	0.274	-0.124

Blocking	11 ± 2	0.319	-0.187

The ability of the modified electrode to detect the CD34 antigen was subsequently investigated. With this purpose, the sensor was incubated with increasing concentrations of the protein in PBS (range: 2.5 - 50 µg mL^{-1}), and then Faradaic EIS responses to each concentration were monitored. As shown in Figure 3, the binding of the protein produces a change in the R_{ct} value, which increases with CD34 concentration. The experimental data are well fitted with the Langmuir equation, $y = y_{max}\, x/ (K_D + x)$, where y_{max} is the saturation response and K_D the dissociation constant. As shown, a maximum signal of 42 ± 2 % was obtained, leading to an estimated dissociation constant of 5.8 ± 0.5 µg mL^{-1} with a correlation of 0.998, demonstrating the excellent selectivity and affinity of the monoclonal antiCD34 antibody that we selected for the construction of the sensor.

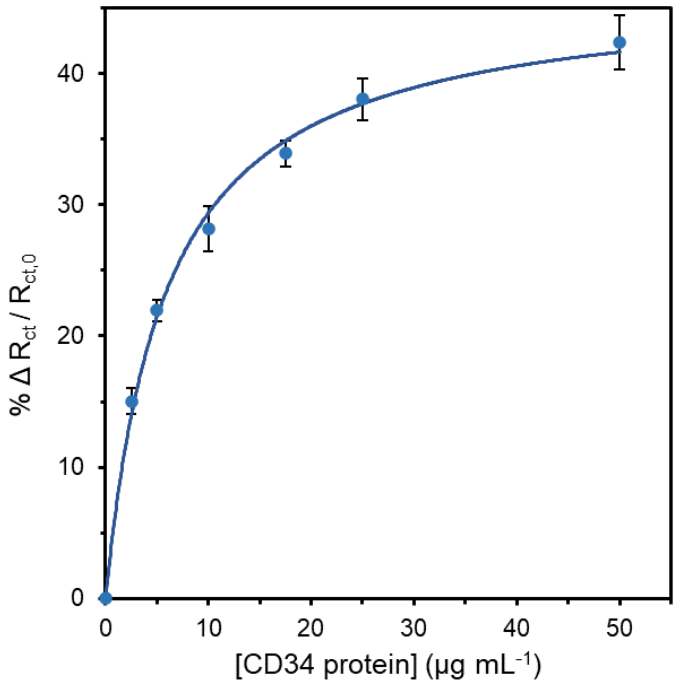

Figure 3: Affinity binding curve of the immobilized anti-CD34 antibody onto the SAM modified screen printed gold electrodes for CD34 protein. The experimental data were

fitted with the Langmuir equation (solid line). Data points refer to experimental data. Error bars refer to three replicates from different electrodes.

The efficacy of the sensor to detect the $CD34^+$ T-cells was subsequently investigated, both in PBS and human serum, under either Faradaic or non-Faradaic conditions. Undiluted serum and increasing dilutions (1:1, 1:5, 1:10, 1:20, 1:50) in PBS were considered. Nonetheless, only from a serum dilution of 1:50 in PBS, an increase on the R_{ct} similar to the one obtained in pure PBS was observed. For all the other dilutions, the value of the R_{ct} increased after the interaction with the cells but the obtained signal was lower than the one for PBS (data not shown).

As shown in Figure 4A, in both PBS and 1:50 diluted serum, the Faradaic EIS measurements revealed an increase of R_{ct} with the concentration of $CD34^+$ T-cells, within the concentration range of 50 – 1 x 10^5 cells mL^{-1}. No significant difference was observed between PBS and diluted human serum. The obtained calibration curves were adjusted to sigmoidal equations, leading to a fitted curve in PBS equal to $y = 37/(1+3.6^{-0.003x})$, and in diluted serum to $y = 34/(1+3.2^{0.002x})$. The linear range, calculated as the concentration range delimited by 10 % of the baseline and 90 % of the saturating cells concentration, resulted to be 210 - 1230 cells mL^{-1} in PBS, and 230 - 1400 cells mL^{-1} in diluted human serum. To further characterize the analytical response of the sensors, the limit of detection was estimated. It was calculated as the concentration corresponding to a signal (% $R_{ct}/R_{ct,0}$) that is the signal of the blank plus three times the standard deviation of the blank (PBS without cells). The limit resulted to be 37 cells mL^{-1} in PBS and 61 cells mL^{-1} in diluted human serum, respectively.

The immunosensor response to each concentration of cells was also investigated according to the non-Faradaic EIS spectra. Capacitive values (C′) at the minimum value for C″, which roughly correspond to the double-layer capacitance values in a Randle's circuit, were used to plot the calibration curve against the concentration of the cells (Figure 4B). The sensor was tested with concentrations of cells between 50 and 1 x 10^5 cells mL^{-1} in PBS and human serum diluted 1:50. As shown, in both media, the capacitive increases linearly in a logarithmic scale with the cell concentrations, within the whole range tested, with a limit of detection of 32 cells mL^{-1} in PBS and 44 cells mL^{-1} in diluted serum. The obtained calibration curves were $y = 2.0054 \cdot \ln(x) - 6.6816$ for PBS buffer, and $y = 1.6512 \cdot \ln(x) - 5.6322$ for diluted human serum, both with a correlation of 0.9997. Thus, demonstrating the capability of measuring directly the binding of $CD34^+$ T-cells to the sensor, without using any redox probe in solution. This result allows the use of the sensor in flow in a microfluidic system.

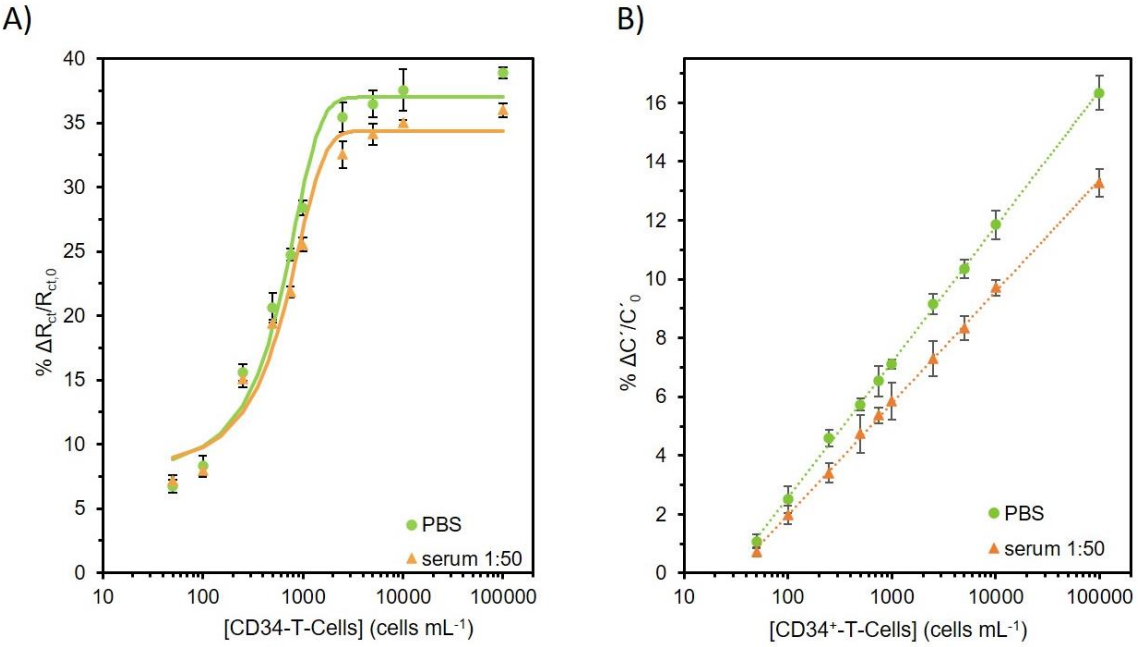

Figure 4: Response of the immunosensor to increasing concentrations of $CD34^+$ T-cells in PBS (green circles) and diluted (1:50) human serum (orange triangles) in logarithmic

scale. A) Calibration curves measured by Faradaic EIS in 5 mM $Fe[(CN)_6]^{3-/4-}$. Data points refer to experimental data and were fitted with a sigmoidal curve. B) Calibration curves obtained by non-Faradaic EIS measurements in PBS and diluted (1:50) human serum. Data points refer to experimental data and were fitted with a logarithmic curve, in both cases, with error bars related to three replicates from independently fabricated sensors.

To the best of our knowledge, this is the first electrochemical immunosensor for $CD34^+$ T-cells detection. So far, only a quartz crystal microbalance immunosensor for $CD34^+$ T-cells has been reported and tested for one concentration of cells only, 500 cells mL^{-1}) [16], while we test the performance of our immunosensor under a wide range of concentrations of $CD34^+$ T-cells. Few electrochemical-based immunosensors for other types of T-cells (e.g. $CD4^+$ and $CD8^+$), have been recently reported, and the analytical characteristics of each of them are summarised in Table 2. Compared to all the immunosensors, the capacitive immunosensor that we report in this study has a wider linear range and a lower limit of detection. Consequently, our immunosensor is a promising tool for the detection of $CD34^+$ T-cells for clinical purposes.

Table 2. Analytical characteristics of immunosensors recently developed for T-cells detection.

T-cell target	**Method of detection**	**Linear range (cell mL^{-1})**	**LOD (cell mL^{-1})**	**Medium**	**Reference**
$CD34^+$	Faradaic EIS	230 - 1400	61	Serum 1:50	This study
$CD34^+$	Capacitive EIS	$50 – 1 \times 10^5$	44	Serum 1:50	This study
$CD34^+$	QCM	-	-	Cellular media	[16]
$CD4^+$	Amperometry	$8.9 \times 10^4 – 9.12$	4.4×10^4	Blood	[17]

		x 10^5			
$CD4^+$	SWV	100 – 1 x 10^6	100	Buffer	[18]
$CD4^+$	Impedance	-	-	Blood	[19]
$CD8^+$	DPV	5 x 10^4 – 6 x 10^6	4 x 10^4	PBS	[20]

To assess the selectivity of the immunosensor developed, several approaches were considered. First, the sensor response to the CD44 protein was investigated. CD44 is a glycoprotein also present on the surface of T-cells. Its length and weight are similar to CD34 protein [21], and therefore it could be a source of non-specific binding to the sensor and a potential interference. Two concentrations of CD44 protein in PBS were considered and the response in terms of Faradaic impedance assessed. Results show that for both concentrations, the percentage of change in the R_{ct} value was 5.6 times lower than the value for the CD34 at 5 µg mL^{-1}, and 5.4 times lower than the value for the CD34 protein at 25 µg mL^{-1} (Figure 5A).

Subsequently, the selectivity of the immunosensor against two other types of cells, C2C12 muscle cells and HL-60 human cells, was investigated. Both C2C12 and HL-60 showed a low expression of CD34 protein (<5 %) confirmed by flow cytometry, which could interfere with the immunosensor reliability (Figure S1). The Faradaic impedimetric response of the sensor to each cell type, at a concentration of 1 x 10^4 cells mL^{-1} in human serum diluted 1:50, was individually investigated. As shown in Figure 5B, the sensor signal towards C2C12 muscle cells was 4.5 times lower than the signal for $CD34^+$ T-cells, and for HL-60 human cells it was 4.9 times lower than the value for $CD34^+$ T-cells. The signal-to-noise (S/N) for $CD34^+$ cells detection is 11 while for the unspecific cells, such as C2C12 and HL60 cells, the S/N is respectively 2.5 and 2.3,

showing the good analytical performance of the developed sensor. Therefore the incubation time with the cells was not further optimized.

To further demonstrate the selectivity of the proposed immunosensor, the response to $CD34^+$ T-cells in the presence of other types of cells (either C2C12 or HL-60) in human serum under different concentration ratios was investigated. In particular, the concentration of $CD34^+$ cells was kept constant at 1000 cells mL^{-1}, while the concentration of C2C12 muscle cells or HL-60 cells, was varied in 1:1, 1:10, and 1:100 ratios. As shown in Figure 5C and 5D, negligible changes in the Faradaic and non-Faradaic impedance measurements are observed for each concentration ratio, thus, demonstrating that the specific binding of $CD34^+$ T-cells to the functionalised immunosensor is not affected by other types of cells that could be present in blood. These results prove the use of the developed immunosensor for clinical applications to specifically detect $CD34^+$ T-cells in serum.

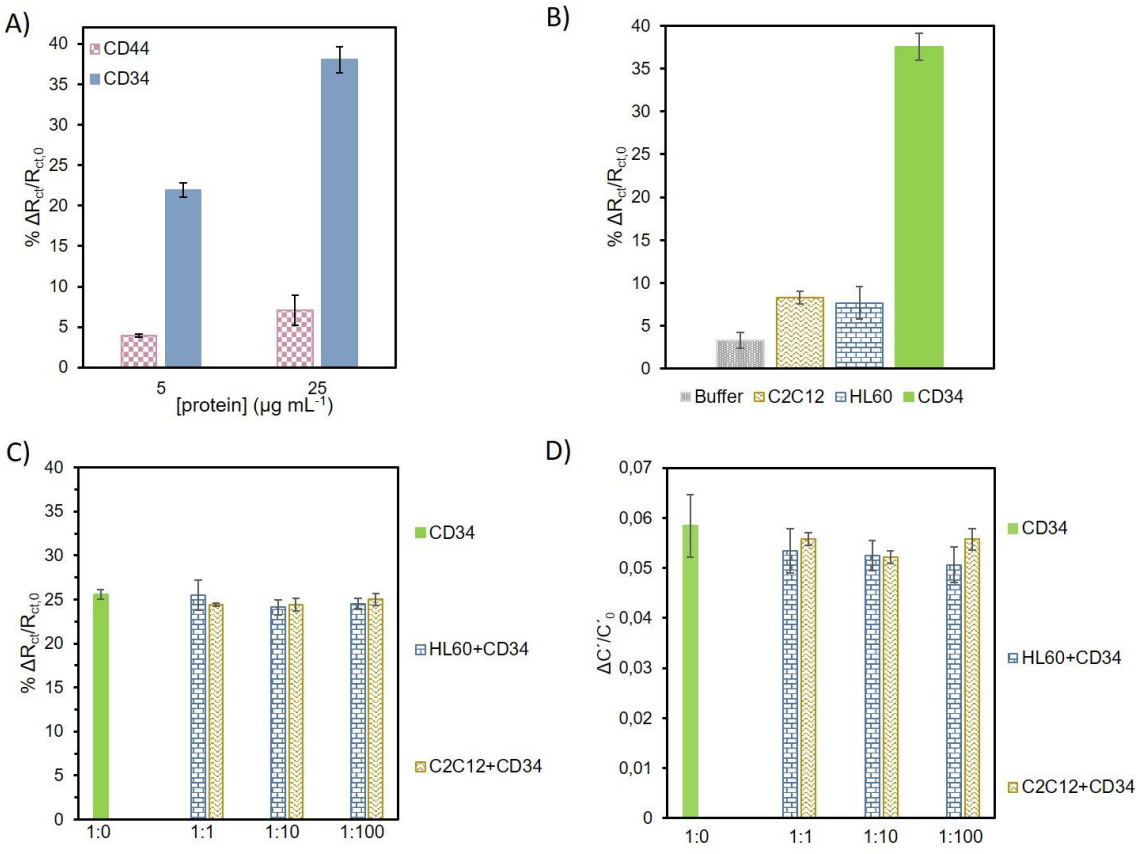

Figure 5: Selectivity of the immunosensor developed. A) Selectivity study against CD44 protein (pink) at two concentrations in PBS compared to the signal obtained for CD34 protein (blue), measured by Faradaic EIS. B) Selectivity against C2C12 (brown) and HL-60 (blue) cells in PBS measured by Faradaic EIS. C) Specific response of the immunosensor for $CD34^+$ cells in the presence of HL-60 (blue) and C2C12 (brown) cells at different concentration ratios measured by Faradaic EIS. D) Specific response of the immunosensor for $CD34^+$ cells in the presence of HL-60 (blue) and C2C12 (brown) cells at different concentration ratios measured by non-Faradaic EIS. Error bars refer to three replicates from independently fabricated sensors.

Finally, the designed immunosensor was fit into a microfluidic system for the continuous capacitive impedance measurements (Figure S2). The system was fed with increasing concentrations of $CD34^+$ T-cells and Figure 6 shows the resulting calibration

curve obtained by plotting the C' value against the concentration of $CD34^+$ T-cells in a logarithmic scale. The correlation is described by the equation y = 0.0167·ln(x) – 0.0531 with a correlation coefficient of 0.9998. As shown, the dynamic range of the immunosensor under flow-through operation is the same than was observed in batch mode, with a limit of detection of 27 cells mL^{-1} (Figure 6). These results demonstrate the applicability of the microfluidic immunosensor to detect $CD34^+$ T-cells in flow-through mode which is compatible with the integration of the sensor into an on-chip detection.

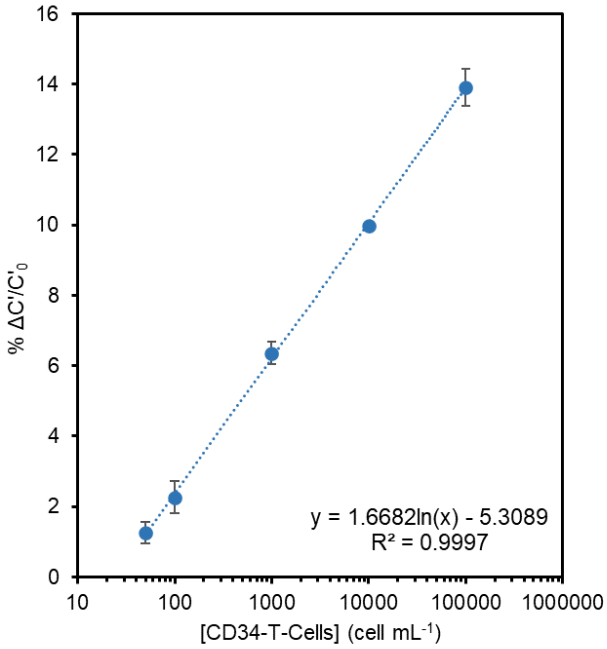

Figure 6: Calibration curve obtained with flow through measurements of the capacitive EIS. Data points refer to experimental data, with error bars related to three replicates from independently fabricated sensors. Data were fitted with a logarithmic curve.

4. Conclusions

Herein, an electrochemical label-free immunosensor for the detection of $CD34^+$ T-cells in diluted human serum was developed. The biosensor, based on a direct assay with a

specific antibody immobilized onto gold electrodes, was employed for the detection of $CD34^+$ T-cells using both Faradaic and non-Faradaic impedance modes. The developed immunosensor shows better analytical characteristics (working range and limit of detection) than the other T-cell electrochemical sensors described in the literature to date. Moreover, our proposed sensor shows excellent selectivity when challenged with other types of cells and similar proteins in serum media. Besides, the electrochemical performance of the developed biosensor remains constant in the presence of other interfering cells in diluted human serum. The developed biosensor was successfully integrated onto a microfluidic system allowing the continuous measurement of the non-Faradaic impedance in PBS. Interestingly, the electrochemical performance of the biosensor in continuous mode is comparable to the static mode in terms of working range, as well as the limit of detection (27 cells mL^{-1}). Consequently, the proposed sensor could be integrated into an on-chip detection for real-time monitoring of the manufacturing process of CAR-T cells. Finally, the immobilization of different antibodies could improve the versatility of the developed platform towards the detection of other types of CAR-T-cells..

CRediT authorship contribution statement

Ana Díaz-Fernández: Investigation, Methodology, Data curation, Writing - original draft, Writing - review & editing. **Elena Bernalte:** Methodology, Writing - review & editing. **Carlos Fernández-Ramos**: Investigation. **Sandhya Moise:** Investigation, Data curation, Writing - review & editing **Pedro Estrela:** Supervision, Writing - review & editing. **Mirella Di Lorenzo:** Conceptualization, Resources, Project administration, Supervision, Writing - review & editing.

Declaration of competing interest

The authors declare no competing financial interest.

Acknowledgments

The authors would like to thank the Engineering and Physical Sciences Research Council (EPSRC) for funding (EP/R022534/1). The authors also thank Scott Allan and Piyanan Boonprasirt for providing the C2C12 and HL-60 cells used in this study.

References

[1] R.L. Siegel, K.D. Miller, A. Jemal, Cancer statistics, 2020, CA. Cancer J. Clin. 70 (2020) 7–30. https://doi.org/10.3322/caac.21590.

[2] F. Bray, J. Ferlay, I. Soerjomataram, R.L. Siegel, L.A. Torre, A. Jemal, Global cancer statistics 2018: GLOBOCAN estimates of incidence and mortality worldwide for 36 cancers in 185 countries, CA. Cancer J. Clin. 68 (2018) 394–424. https://doi.org/10.3322/caac.21492.

[3] S. Feins, W. Kong, E.F. Williams, M.C. Milone, J.A. Fraietta, An introduction to chimeric antigen receptor (CAR) T-cell immunotherapy for human cancer, Am. J. Hematol. 94 (2019) S3–S9. https://doi.org/10.1002/ajh.25418.

[4] S.A. Grupp, M. Kalos, D. Barrett, R. Aplenc, D.L. Porter, S.R. Rheingold, D.T. Teachey, A. Chew, B. Hauck, J.F. Wright, M.C. Milone, B.L. Levine, C.H. June, Chimeric Antigen Receptor–Modified T Cells for Acute Lymphoid Leukemia, N. Engl. J. Med. 368 (2013) 1509–1518. https://doi.org/10.1056/nejmoa1215134.

[5] S.L. Maude, T.W. Laetsch, J. Buechner, S. Rives, M. Boyer, H. Bittencourt, P. Bader, M.R. Verneris, H.E. Stefanski, G.D. Myers, M. Qayed, B. De Moerloose, H. Hiramatsu, K. Schlis, K.L. Davis, P.L. Martin, E.R. Nemecek, G.A. Yanik, C.

Peters, A. Baruchel, N. Boissel, F. Mechinaud, A. Balduzzi, J. Krueger, C.H. June, B.L. Levine, P. Wood, T. Taran, M. Leung, K.T. Mueller, Y. Zhang, K. Sen, D. Lebwohl, M.A. Pulsipher, S.A. Grupp, Tisagenlecleucel in Children and Young Adults with B-Cell Lymphoblastic Leukemia, N. Engl. J. Med. 378 (2018) 439–448. https://doi.org/10.1056/nejmoa1709866.

[6] T.I. Panagopoulou, Q.A. Rafiq, CAR-T immunotherapies: Biotechnological strategies to improve safety, efficacy and clinical outcome through CAR engineering, Biotechnol. Adv. 37 (2019) 107411. https://doi.org/10.1016/j.biotechadv.2019.06.010.

[7] K.C. Pehlivan, B.B. Duncan, D.W. Lee, CAR-T Cell Therapy for Acute Lymphoblastic Leukemia: Transforming the Treatment of Relapsed and Refractory Disease, Curr. Hematol. Malig. Rep. 13 (2018) 396–406. https://doi.org/10.1007/s11899-018-0470-x.

[8] B. Fehse, A. Richters, K. Putimtseva-Scharf, H. Klump, Z. Li, W. Ostertag, A.R. Zander, C. Baum, CD34 Splice Variant: An Attractive Marker for Selection of Gene-Modified Cells, Mol. Ther. 1 (2000) 448–456. https://doi.org/10.1006/mthe.2000.0068.

[9] P. Salvo, F.M. Vivaldi, A. Bonini, D. Biagini, F.G. Bellagambi, F.M. Miliani, F. Di Francesco, T. Lomonaco, Biosensors for Detecting Lymphocytes and Immunoglobulins, Biosensors. 10 (2020) 1–19. https://doi.org/10.3390/bios10110155.

[10] N. Bhalla, P. Jolly, N. Formisano, P. Estrela, Introduction to biosensors, Essays Biochem. 60 (2016) 1–8. https://doi.org/10.1042/EBC20150001.

[11] F.S. Felix, L. Angnes, Electrochemical immunosensors – A powerful tool for analytical applications, Biosens. Bioelectron. 102 (2018) 470–478.

https://doi.org/10.1016/j.bios.2017.11.029.

[12] F. Fathi, R. Rahbarghazi, M.R. Rashidi, Label-free biosensors in the field of stem cell biology, Biosens. Bioelectron. 101 (2018) 188–198. https://doi.org/10.1016/j.bios.2017.10.028.

[13] J.L. Hammond, N. Formisano, P. Estrela, S. Carrara, J. Tkac, Electrochemical biosensors and nanobiosensors, Essays Biochem. 60 (2016) 69–80. https://doi.org/10.1042/EBC20150008.

[14] E.B. Bahadir, M.K. Sezgintürk, A review on impedimetric biosensors, Artif. Cells, Nanomedicine Biotechnol. 44 (2016) 248–262. https://doi.org/10.3109/21691401.2014.942456.

[15] X. Luo, J.J. Davis, Electrical biosensors and the label free detection of protein disease biomarkers, Chem. Soc. Rev. 42 (2013) 5944–5962. https://doi.org/10.1039/c3cs60077g.

[16] O. Maglio, S. Costanzo, R. Cercola, G. Zambrano, M. Mauro, R. Battaglia, G. Ferrini, F. Nastri, V. Pavone, A. Lombardi, A quartz crystal microbalance immunosensor for stem cell selection and extraction, Sensors (Switzerland). 17 (2017) 1–14. https://doi.org/10.3390/s17122747.

[17] S. Carinelli, C. Xufré Ballesteros, M. Martí, S. Alegret, M.I. Pividori, Electrochemical magneto-actuated biosensor for CD4 count in AIDS diagnosis and monitoring, Biosens. Bioelectron. 74 (2015) 974–980. https://doi.org/10.1016/j.bios.2015.07.053.

[18] J. Kim, G. Park, S. Lee, S.W. Hwang, N. Min, K.M. Lee, Single wall carbon nanotube electrode system capable of quantitative detection of CD4+ T cells, Biosens. Bioelectron. 90 (2017) 238–244. https://doi.org/10.1016/j.bios.2016.11.055.

[19] N.N. Mishra, S. Retterer, T.J. Zieziulewicz, M. Isaacson, D. Szarowski, D.E. Mousseau, D.A. Lawrence, J.N. Turner, On-chip micro-biosensor for the detection of human CD4+ cells based on AC impedance and optical analysis, Biosens. Bioelectron. 21 (2005) 696–704. https://doi.org/10.1016/j.bios.2005.01.011.

[20] D. Sun, X. Zheng, W. Yang, X. Xie, X. Yang, Electrochemical immunosensor for CD8+ T-cells based on a functionalized multi-walled carbon nanotubes-modified electrode, Anal. Methods. 5 (2013) 5248–5252. https://doi.org/10.1039/c3ay41057a.

[21] D.B. Abusamra, F.A. Aleisa, A.S. Al-Amoodi, H.M.J. Ahmed, C.J. Chin, A.F. Abuelela, P. Bergam, R. Sougrat, J.S. Merzaban, Not just a marker: CD34 on human hematopoietic stem/progenitor cells dominates vascular selectin binding along with CD44, 1 (2017) 2799–2816. https://doi.org/10.1182/bloodadvances.2017004317.

Supplementary Information

An impedimetric immunosensor for the selective detection of $CD34^+$ T-cells in human serum

Ana Díaz-Fernández[1,2], Elena Bernalte[1,2], Carlos Fernández-Ramos[1], Sandhya Moise[1,2], Pedro Estrela[2,3], Mirella Di Lorenzo[1,2,*]

[1] Department of Chemical Engineering, University of Bath, Bath, BA2 7AY, United Kingdom

[2] Centre for Biosensors, Bioelectronics and Biodevices (C3Bio), University of Bath, BA2 7AY, Bath, United Kingdom.

[3] Department of Electronic and Electrical Engineering, University of Bath, BA2 7AY, Bath, United Kingdom

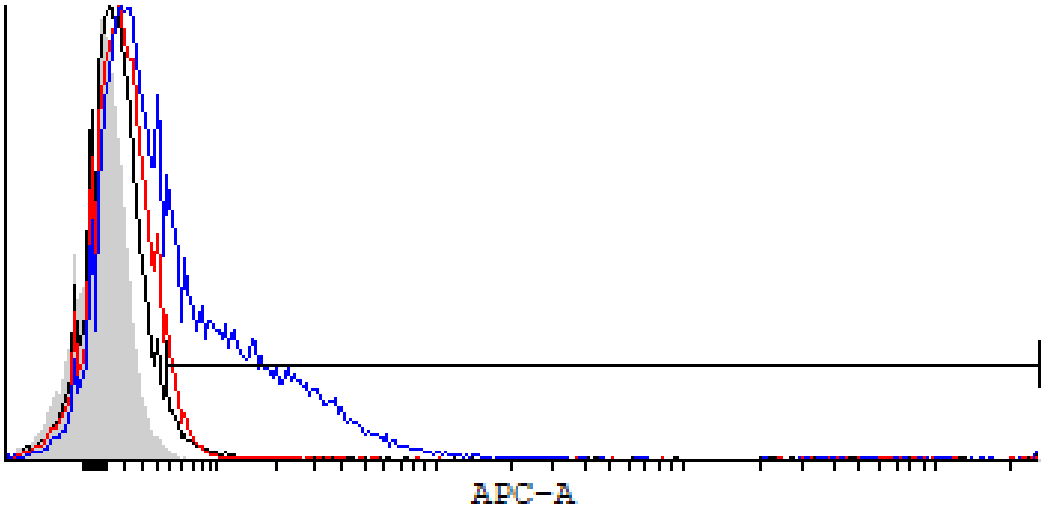

Figure S1: Histogram overlay shows $CD34^{+}$ PBMCs (blue line) showing a higher expression of the CD34 marker compared to the C2C12 myoblast cells (black line) and HL-60 leukemia cells (red line). The grey filler plot indicates the background fluorescence of IgG1-stained PBMCs.

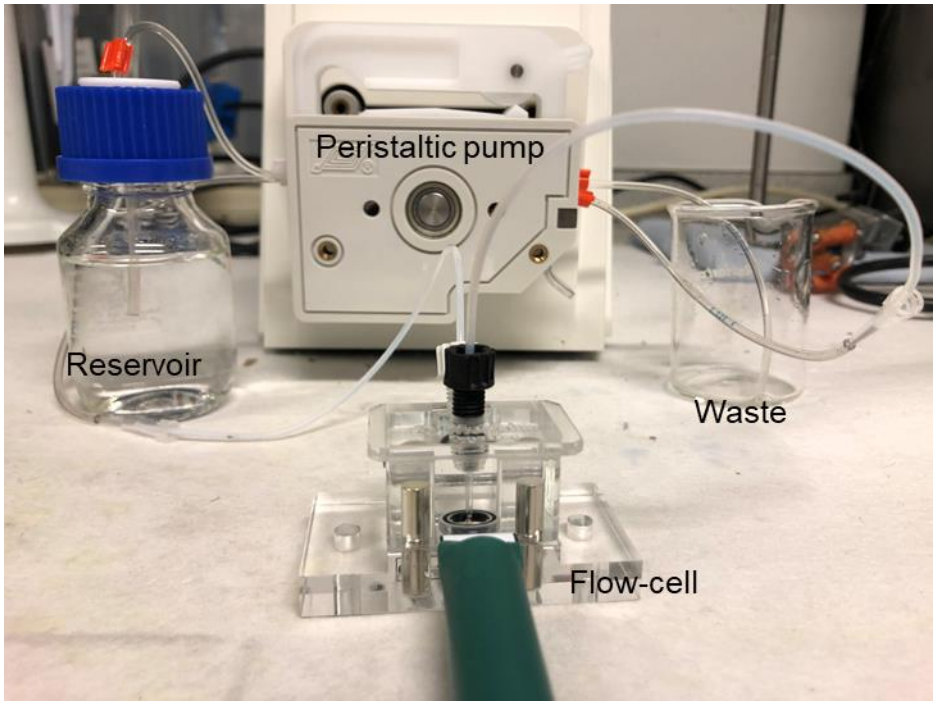

Figure S2: Experimental set-up for the flow-through tests